

## Synthesis Design

## A New, Simple and Versatile Strategy for the Synthesis of Short Segments of Zigzag-Type Carbon Nanotubes

Etienne André,<sup>[a]</sup> Baptiste Boutonnet,<sup>[a]</sup> Pauline Charles,<sup>[a]</sup> Cyril Martini,<sup>[a]</sup> Juan-Manuel Aguiar-Hualde,<sup>[b]</sup> Sylvain Latil,<sup>[b]</sup> Vincent Guérineau,<sup>[c]</sup> Karim Hammad,<sup>[c]</sup> Priyanka Ray,<sup>[a]</sup> Régis Guillot,<sup>[a]</sup> and Vincent Huc<sup>\*[a]</sup>

**Abstract:** Short segments of zigzag single-walled carbon nanotubes (SWCNTs) were obtained from a calixarene scaffold by using a completely new, simple and expedited strategy that allowed fine-tuning of their diameters. This new approach also allows for functionalised short segments of zigzag SWCNTs to be obtained; a prerequisite towards their

lengthening. These new SWCNT short segments/calixarene composites show interesting behaviour in solution. DFT analysis of these new compounds also suggests interesting photophysical behaviour. Along with the synthesis of various SWCNTs segments, this approach also constitutes a powerful tool for the construction of new, radially oriented  $\pi$  systems.

## Introduction

The rediscovery<sup>[1]</sup> of carbon nanotubes (CNTs) by Iijima in 1991,<sup>[2]</sup> and most importantly the discovery of single-walled carbon nanotubes (SWCNTs) by Iijima and Ichihashi<sup>[3]</sup> and Kiang<sup>[4]</sup> in 1993, opened up a new world in chemistry and physics, especially regarding electron transport characteristics at the nanoscale.<sup>[5–7]</sup> It was shown that the electronic behaviour of SWCNTs was directly related to the way in which the constituting graphene sheet was rolled.<sup>[8]</sup> So far, most known syntheses of CNTs offer a limited degree of control over this rolling process.<sup>[9–12]</sup> Post-synthesis sorting processes are thus required.<sup>[13–16]</sup> A radical solution would be the total synthesis of CNTs through synthetic organic chemistry.

With few exceptions,<sup>[17–19]</sup> most of the experimental approaches developed so far for the synthesis of SWCNTs are directed towards the synthesis of armchair-type nanotubes.<sup>[20–38]</sup> All of these tubes will be metallic, regardless of their diameter.<sup>[8]</sup> Conversely, a diameter-controlled strategy, for the synthesis of zigzag CNTs would open up the way to both metallic and semiconducting nanotubes. Indeed, it was shown that the electronic properties of zigzag nanotubes were solely dependent on their diameters.<sup>[8]</sup> Most of the proposed strategies to-

wards the synthesis of zigzag CNTs are based on cyclacene-type repeating units as a starting point (Figure 1 A). Because the synthesis of these long-pursued compounds is still elusive, we decided to consider a different approach.

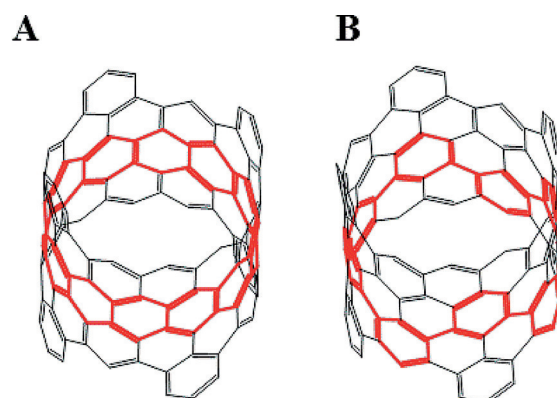


**Figure 1.** Topological representation of cyclacene (A) and cyclo[n](m-phenylene) (B) repeating units for the total synthesis of zigzag SWCNTs.

Analysis of the structure of zigzag CNTs led us to conclude that a different repeating unit, namely, cyclo[n](m-phenylene) (CMP),<sup>[39–42]</sup> could also be considered as an interesting starting point (Figure 1 B).

Reports in the literature (along with molecular modelling) shows that CMPs exhibit planar or saddle-like geometries.<sup>[39–43]</sup> This definitively precludes their direct use as a starting point for the synthesis of radially conjugated compounds, such as CNTs. It is thus necessary to constrain the geometry of these macrocycles to force them to adopt a “tubular” geometry, closer to the final radially oriented  $\pi$  system of the target CNTs. Herein, we report the first experimental steps towards

[a] Dr. E. André, Dr. B. Boutonnet, P. Charles, Dr. C. Martini, Dr. P. Ray, Dr. R. Guillot, Dr. V. Huc  
Institut de Chimie Moléculaire et Matériaux d'Orsay (ICMMO)  
15 rue Georges Clémenceau, 91405 Orsay (France)  
E-mail: Vincent.huc@u-psud.fr

[b] Dr. J.-M. Aguiar-Hualde, Dr. S. Latil  
CEA Saclay - Orme des Merisiers  
91191 Gif-sur-Yvette Cedex (France)

[c] V. Guérineau, K. Hammad  
Institut de Chimie des Substances Naturelles (ICSN)  
CNRS, 91300 Gif-Sur-Yvette Cedex (France)

Supporting information for this article is available on the WWW under <http://dx.doi.org/10.1002/chem.201503693>.

the synthesis of zigzag CNTs with a priori well-defined diameters by using this completely new CMP-based approach.

An extensive NMR spectroscopy analysis of these new calixarene-scaffolded zigzag SWCNT short segments demonstrated their cyclic structure. It also showed that these compounds exhibited complex dynamic behaviour in solution. These structural characterisations were supported by DFT analysis.

## Results and Discussion

Our strategy relies on the use of conformationally locked calix[4]arene, calix[5]arene and calix[6]arene as scaffolds to build the corresponding zigzag SWCNTs (Figure 2).

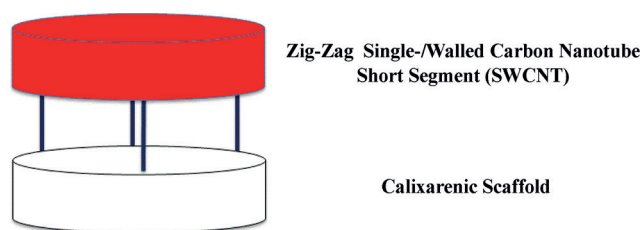


Figure 2. The calixarene/SWCNT composites described herein.

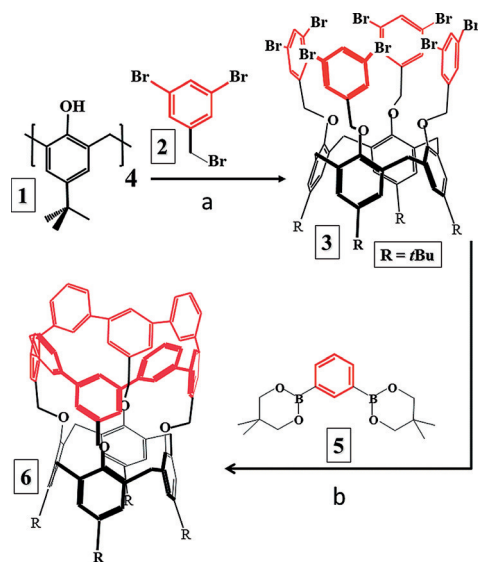


Figure 3. Two-step synthesis of the cyclo[8](*m*-phenylene)-type SWCNT segment on a calix[4]arene scaffold (6). Reagent and conditions: a) THF/DMF/NaH,  $-78^{\circ}\text{C} \rightarrow \text{RT}$ , overnight; b) 5,  $[\text{Pd}(\text{PPh}_3)_4]$ , CsF, dioxane, reflux, 10 h.

As shown in Figures 3, 4, and 5, the proposed strategy is general and has been successfully applied to different calixarene platforms. It relies on the synthesis of key poly-halogenated scaffolds of different diameters (compounds 3, 8, 14 and 19) starting from the corresponding calixarenes 1, 7 and 10.

The poly-halogenated calixarene scaffolds 3, 8, 14 and 19 are then subjected to cascade Suzuki couplings to introduce the missing aromatic units required for the target SWCNT short segments.<sup>[2]</sup>

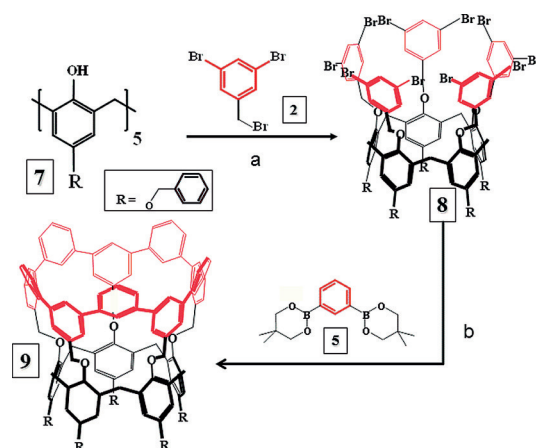


Figure 4. Two-step synthesis of a cyclo[10](*m*-phenylene)-type SWCNT segment on a calix[5]arene scaffold (9). Reagent and conditions: a) 2,  $\text{CH}_3\text{CN}$ ,  $\text{K}_2\text{CO}_3$ , overnight; b) 5,  $[\text{Pd}(\text{PPh}_3)_4]$ , CsF, dioxane, reflux, 6 h.

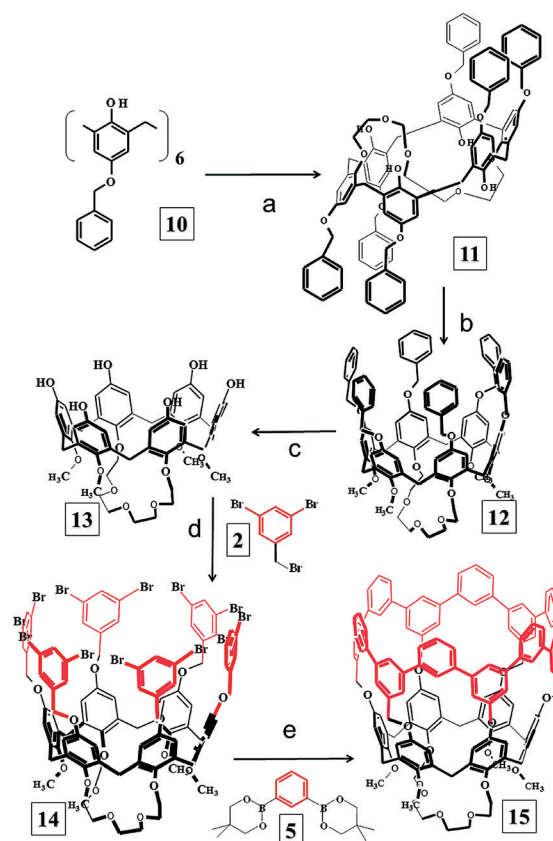


Figure 5. Five-step synthesis of the cyclo[12](*m*-phenylene)-type SWCNT segment from a calix[6]arene scaffold (15). Reagent and conditions: a) triethyleneglycol bis(tosylate), *t*BuOK, toluene,  $100^{\circ}\text{C}$  overnight; b) MeI, DMF, RT, overnight;<sup>[45]</sup> c)  $\text{Pd}(\text{OH})_2/\text{C}$ ,  $\text{H}_2$ , 48 h; d) 2, THF/DMF  $50^{\circ}\text{C}$ , overnight; e) 5,  $[\text{Pd}(\text{PPh}_3)_4]$ , CsF, dioxane, reflux, 6 h.

### Synthesis of the poly-halogenated calixarene scaffolds

Regarding the synthesis of 6 (Figure 3), calixarene scaffold 3 is obtained from commercially available *p*-*tert*-butylcalix[4]arene 1 by NaH-promoted alkylation, by using the commercially available 3,5-(dibromo)(bromomethyl)benzene (2).<sup>[45]</sup>

We observed that the proportion of expected cone derivative **3** (Figure S1a–d in the Supporting Information) versus partial cone derivative **4** (Figure S2a–d in the Supporting Information) dramatically increased at low temperature. Starting the reaction at  $-78^{\circ}\text{C}$  resulted in 90% yield of scaffold **3**. This compound was fully characterised by  $^1\text{H}/^{13}\text{C}$  NMR spectroscopy and mass spectrometry (Figure S1a–d in the Supporting Information). The  $^1\text{H}$  NMR spectrum is especially informative: the cone conformation of **3** is demonstrated by the presence of a characteristic pair of doublets (at  $\delta=2.8$  and 3.95 ppm), which corresponds to the bridging methylene groups.

Regarding the synthesis of **9** (Figure 4), the key cone-locked decabromo derivative scaffold **8** was obtained by direct alkylation of the starting *p*-(benzyloxy)calix[5]arene<sup>[46,47]</sup> in acetonitrile. The presence of the cone conformer was demonstrated by both  $^1\text{H}$  NMR spectroscopy experiments (Figure S5 in the Supporting Information) and single-crystal XRD analysis (Figure 6 and Figures S5a and S19 in the Supporting Information).

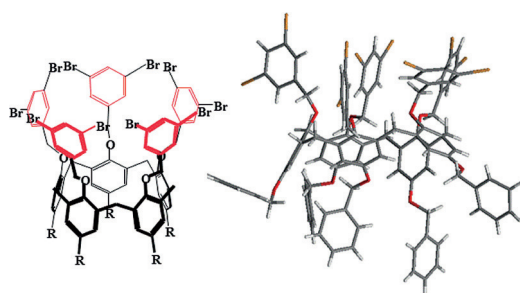


**Figure 6.** Structural determination of the (decabromo)calix[5]arene scaffold **8** by X-ray diffraction (R = benzyloxy). Colour code: H, white; C, black; O, red; Br, brown.

Regarding the synthesis of the calix[6]arene-derived SWCNT short segment **15**, (Figure 5), the synthesis of the dodecabinated scaffold **14** was more complex than the two previous cases. Indeed, locking the starting *p*-(benzyloxy)calix[6]arene **10**<sup>[46,47]</sup> in the cone conformation requires the two-step pre-organisation sequence depicted in Figure 5.<sup>[44]</sup> Compound **10** was first alkylated by triethyleneglycol bis(tosylate) (step a in Figure 5), and then by methyl iodide (step b in Figure 5). During this second alkylation process, a conformational switch is observed from alternate (**11**) to cone (**12**).<sup>[44]</sup> Debenzylation of the resulting cone-shaped platform **12** quantitatively resulted in **13**, which was then alkylated in nearly quantitative yields with commercially available **2**. The resulting (dodecabinato)-calix[6]arene precursor **14** is easily obtained on a 10 g scale (Figure S10 in the Supporting Information).

### Assembly of the SWCNT short segments by cascade Suzuki couplings

The final Suzuki-type coupling step required extensive optimisation work with all of the previously described polybrominated scaffolds. Regarding the first SWCNT short seg-

ment (**6**), only a combination of CsF in dioxane, along with  $[\text{Pd}(\text{PPh}_3)_4]$ <sup>[48]</sup> finally allowed us to obtain **6** in 4% yield (Figure S4 in the Supporting Information). Surprisingly, by using the same conditions with the calix[5] and -[6]-derived scaffolds **8** and **14**, no detectable amounts of the expected segments **9** and **15** were obtained. A second extensive optimisation procedure finally allowed us to obtain these compounds in 4 and 1% yield, respectively. Albeit low, these yields compare with those described for the first synthesis of cyclo-*p*-poly(phenylene)s by Jasti et al.<sup>[20]</sup> (ranging from 0.2 to 1.4%). Interestingly, the catalytic conditions optimised for **9** and **15** are quite different from those used to obtain **6**. A 10-fold increase in the amount of catalyst proved to be necessary (to accelerate the reaction; thus reducing debrominations/deborylations), along with a 10-fold dilution of the reaction medium (to reduce the number of Suzuki over-couplings; see Figures S4j, S11s and S6r in the Supporting Information). However, once optimised, the purification of **9** and **15** is surprisingly easy, considering that more than 50 calixarene-derived by-products are observed in both cases in the crude samples (Figures S6q and S11p in the Supporting Information). Purification only involves three successive washing steps with suitable solvents and a final preparative TLC step (Figures S6a and S11a in the Supporting Information). Interestingly, this purification protocol is very similar in both cases, despite the very different functionalisation patterns of **9** and **15**. This shows that the behaviour of these compounds during purification is mostly determined by the upper SWCNT short segment annulus. This may be due to the rigidification effect associated with the presence of the closed SWCNT upper segment, in sharp contrast with the more flexible acyclic by-products.

### Characterisation of the zigzag SWCNT short segments

Compounds **6**, **9**, **15** and **20** are the first examples of diameter-controlled short segments of zigzag SWCNTs. They were fully characterised by mass spectrometry and a combination of 1D and 2D NMR spectroscopy experiments (see Figures S4a–i, S6a–r, S11a–r and S13–S17 in the Supporting Information). The  $^1\text{H}$  NMR spectra of **9**, **6** and **12** are especially exotic, and clearly demonstrate the tubular structure of these products (Figures 7 to 14, below).

Regarding segment **6**, the  $^1\text{H}$  NMR spectrum is symmetric, as expected. The preservation of the cone conformation of the lower calixarene stage is evidenced by the presence of characteristic bridging methylene doublets. This implies that the upper cyclophenylene unit adopts a tubular shape. Very high chemical shifts are observed for the bridging methylene protons (Figure 7, green hydrogen atoms). Those protons are observed at  $\delta=5$  and 3.7 ppm, which is shifted by +0.5 ppm relative to most previously described calix[4]arene derivatives in the same cone conformation.<sup>[45]</sup> This effect is attributed to the convergent influences of the deshielding cone of the three surrounding phenyl units (green arrows).

Conversely, the methylene protons from the benzyl groups (Figure 7, blue hydrogen atoms) are observed at  $\delta=4.2$  ppm, which is shielded by nearly 1 ppm compared with its usual

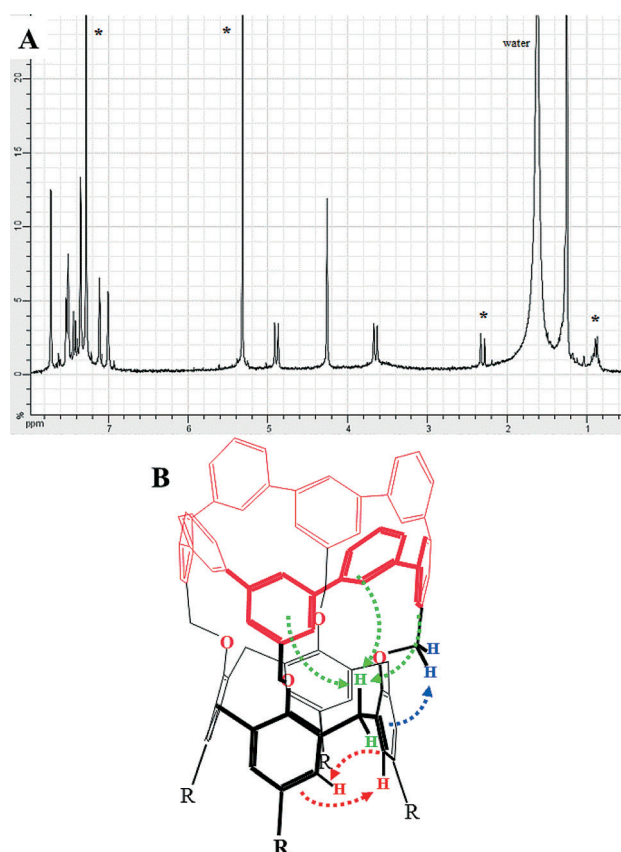


**Figure 7.** A)  $^1\text{H}$  NMR spectra of **6** (solvents marked with asterisks) and B) influence of the presence of the cyclo[8](*m*-phenylene) stage on the chemical shifts of the calixarene protons. The magnetic influence of the aromatic groups on the chemical shifts of some protons is indicated by arrows.

value ( $\delta \approx 5$  ppm). This effect is attributed to the proximity of the shielding cone of the aromatic groups from the calix[4]arene lower stage (Figure 7, blue arrow).

A third piece of structural information provided by  $^1\text{H}$  NMR spectroscopy is the deshielding effect observed for the aromatic hydrogen atoms from the calixarene scaffold (Figure 7, red hydrogen atoms). These are shifted by +0.5 ppm compared with their usual values ( $\delta \approx 7$  ppm), due to the reduction of the cone angle of the calixarene lower stage upon the formation of the upper *m*-(phenylene) macrocycle. The two aromatic protons are then brought in close proximity, which increases the influence of the deshielding cone from the neighbouring aromatic moiety (Figure 7, red arrows). Lastly, NOESY analysis (Figures S4g–i in the Supporting Information) also confirmed the cylindrical shape of **6**. Indeed, the NOESY spectrum shows the expected through-space couplings between the protons from the SWCNT stage.

Regarding segment **9**, the  $^1\text{H}$  NMR spectrum is surprisingly complex (Figure 8A and Figure S6c in the Supporting Information). This shows that a symmetry-lowering effect occurs, which is not observed with **6**. Careful examination of the spectrum shows the presence of a characteristic pattern of three signals tentatively associated with an aromatic group, but shifted upfield by 2 ppm compared with the others aromatic groups (Figure 8A, red asterisks (magnification in the inset)).

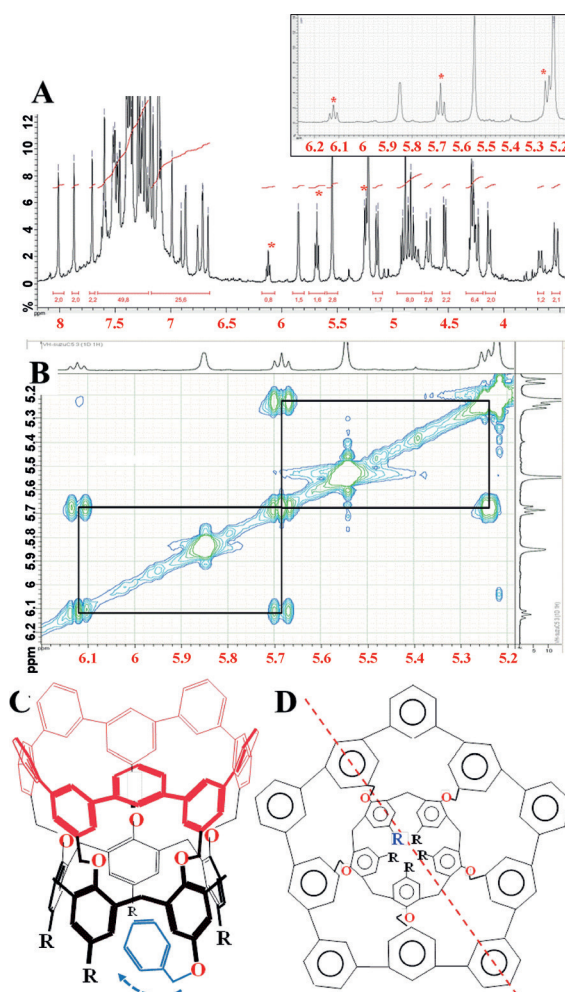


**Figure 8.** A)  $^1\text{H}$  NMR spectrum of the SWCNT short segment/calixarene composite **9** (signals from the self-included phenyl group are marked with red asterisks; inset: magnification of these signals). B) COSY analysis provides evidence of coupling between the protons of the included phenyl group. C) The self-inclusion phenomenon affecting one benzyloxy group is highlighted by the blue arrow. D) In-plane projection of **9** (top view), highlighting its symmetry plane ( $R = \text{benzyloxy}$ ). The self-included benzyloxy groups is highlighted in blue.

This interpretation was first confirmed by COSY analysis (Figure 8B and Figure S6j in the Supporting Information), which showed that these three signals were indeed coupled. Lastly, HSQC analysis (Figure S6i in the Supporting Information) shows that these three signals are associated with phenyl-type carbon atoms (characteristic chemical shifts at  $\delta \approx 130$  ppm).

This upfield shift phenomenon is characteristic of an inclusion process inside the calixarene cavity. Indeed, it was shown that such an inclusion process places the guest in the convergent shielding cone of all the aromatic groups of the calixarene host.<sup>[49]</sup> As the intensity of the signals of the included aromatic group corresponds to exactly one aromatic group (Figure 8A), this led us to conclude that one of the benzyloxy legs of the molecule was self-included inside the lower-stage calixarene cavity (Figure 8C, blue).

This self-inclusion phenomenon results in a symmetry plane crossing the molecule (Figure 8D, red dotted line).  $^1\text{H}/^{13}\text{C}$  NMR

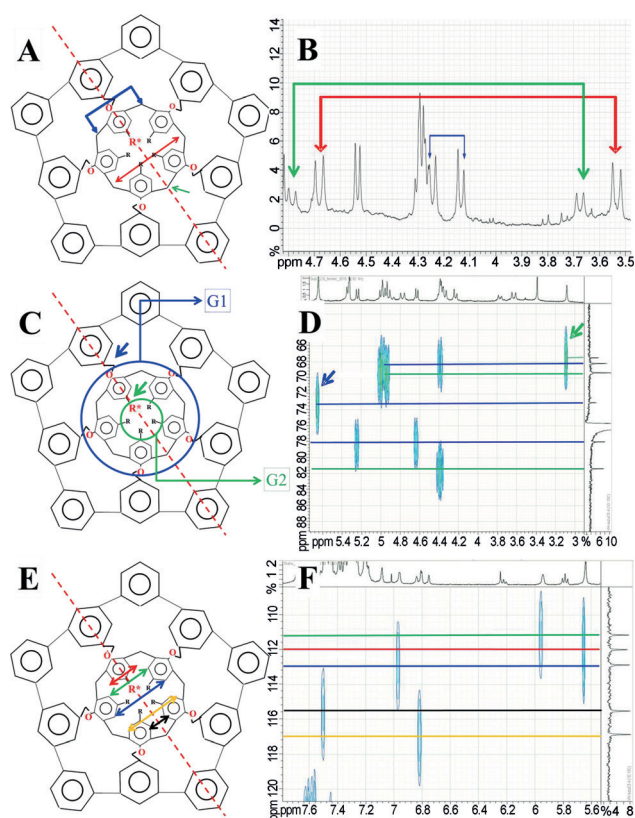


**Figure 9.** Expected (A) and observed (B) patterns for the bridging methylene area of **9** (calixarene scaffold) in the  $^1\text{H}$  NMR spectrum. The three doublets are highlighted with blue, red and green arrows. C) Expected pattern for the benzyloxy groups. The blue and green circles highlight the two sets of benzyloxy groups in **9**. D) Magnification of the benzyloxy area of the HSQC experiment. The blue/green arrows highlight the two benzyloxy groups that appear as singlets. E) Expected pattern for the hydroquinone groups. F) Magnification of the hydroquinone groups area of the HSQC experiment.

spectroscopy analysis of **9** is fully consistent with the aforementioned results (Figure 9). Three doublets in an expected intensity ratio of 2/2/1 (Figure 9A) are observed (Figure 9B) for the bridging methylenes of the calixarene scaffold (highlighted as blue, red and green arrows in Figure 9).

In the same way, six different benzyloxy-type groups are expected (Figure 9C) and observed (Figure 9D and Figure S6g in the Supporting Information;  $^{13}\text{C}$  chemical shifts at  $\delta \approx 80$  ppm). Indeed, compound **9** exhibits two sets of such groups, each including three inequivalent benzyloxy bonds. The first set links the SWCNT stage to the calixarene one (Figure 9C, G1), and the second one belongs to the calixarene stage (Figure 9C, G2). Two of these benzyloxy groups appear as singlets (Figure 9C and D, green/blue arrows) because they are crossed by the symmetry plane.

Lastly, five hydroquinone-type protons are expected (Figure 9E) and observed (Figure 9F and Figures S6h in the Supporting Information), with characteristic  $^{13}\text{C}$  chemical shifts falling in the  $\delta = 112\text{--}120$  ppm range. All of these analysis are perfectly confirmed by COSY experiments (Figure S6k–m in the Supporting Information), which in each case show the expected coupling patterns. All of these previously described NMR

spectroscopy analyses are also fully supported by HMBC (Figure S6n in the Supporting Information) and ROESY (Figure S6o and p in the Supporting Information) experiments.

The identity and purity of the product were further confirmed by mass spectrometry. Figure S6q in the Supporting Information shows the MALDI mass spectra ( $\text{Cs}^+$  cationised) of the same sample as that used for the previously described NMR spectroscopy experiments. Only one single signal is observed. Accordingly, TLC analysis of this sample shows only a single spot.

The self-inclusion phenomenon of a benzyloxy group inside the calixarene cavity of **9** is not observed for **8** because, even if the latter exists in the cone conformation, it is still quite a flexible compound. This results in large fluctuations of the diameter/shape of the calix[5]arene cavity. This reduces fitting between the aromatic cavity of the calixarene and benzyloxy group; thus lowering the association constant.

In the case of **9**, the calixarene structure is made extremely rigid by the presence of the SWCNT short segment. This pre-organises and reduces the size of the cavity, and thus, reinforces the inclusion of the benzyloxy leg.

This phenomenon can be considered as characteristic of the rigidification of the calixarene cavity (i.e., of the successful assembly of the SWCNT short segment), and thus, confirms the structure of **9**.

Regarding the SWCNT short segment/calixarene composite **15**, analysis of the  $^1\text{H}$  NMR spectrum proved to be more difficult and revealed complex dynamic behaviour in solution. The ambient-temperature  $^1\text{H}$  NMR spectrum of **15** in  $\text{CDCl}_3$  is shown in Figure 10A (see also Figure S11b in the Supporting Information). Only broad, ill-defined features are observed.

We suggest that this phenomenon results from slow rotations (at ambient temperature) of the upper nanotube segment versus the lower calixarene stage (Figure 10C, blue arrows), due to rotation around the benzyloxy bonds. Indeed, analysis of molecular models shows that the  $\text{Ar-O-CH}_2$  benzylic bonds linking the two macrocyclic stages are almost free to rotate (Figure 10C, green arrows). This quasi-absence of any defined signals at ambient temperature made it extremely difficult to track the product during the early design of its purification procedure.

To confirm this interpretation, both low- and high-temperature NMR experiments were undertaken. Due to the limited stability of **15** at high temperatures (see below), we first performed the NMR spectroscopy analysis at low temperature to slow down and stop the rotational motion depicted in Figure 10C. As expected, we observed the progressive appearance of sharp signals as the temperature decreased (Figure S11c in the Supporting Information), showing the existence of a well-defined, low-symmetry conformation at 233 K (Figure 10B and Figure S11c in the Supporting Information). This temperature was chosen for the subsequent low-temperature analysis as the best compromise between different trends: 1) easily observed, sharp signals; 2) sufficient signal-to-noise ratio; 3) no precipitation; and 4) no freezing of the solvent. Indeed, at 233 K, the solution of **15** in chloroform is nearly saturated, and we are close to the freezing point of this solvent.

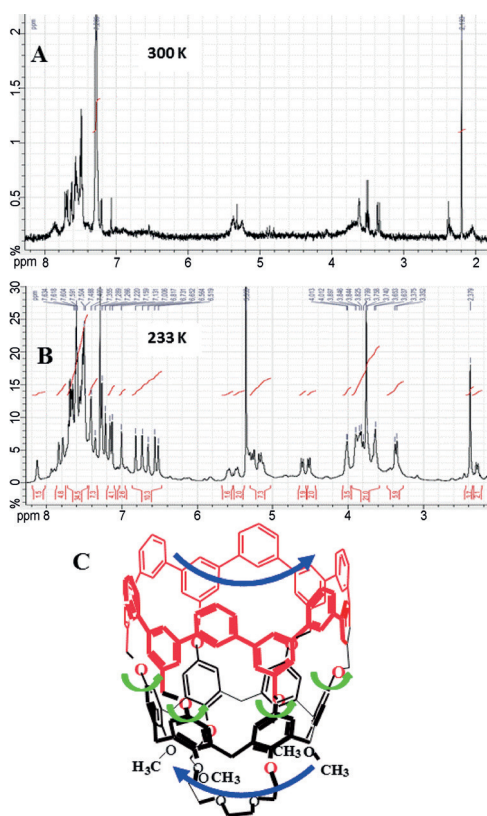


**Figure 10.** A) Ambient- and B) low-temperature  $^1\text{H}$  NMR spectroscopy analyses of **15**. C) Rotational motion of the two macrocyclic stages (blue arrows) around the benzyloxy bonds (green arrows) at room temperature.

According to DFT calculations, the most stable conformer of **15** shows the calixarene stage and the SWCNT short segment “twisted” together (Figure 11 A, side view, and B, top view, see also Figure S18 in the Supporting Information). Figure 11 C shows a simplified top view (i.e. in plane projection) of this conformation, depicting this twist. This conformation shows a pseudo-symmetry axis, crossing the centre of the molecule, and running perpendicular to the drawing (Figure 11 C, yellow cross).

At 233 K, NMR spectroscopy analysis is fully consistent with this structure (Figure 12). As expected, six doublets are observed for the bridging methylenes belonging to the calixarene stage (Figure 12 A and B, red arrows; and Figure S11d and e in the Supporting Information). This was confirmed by 2D COSY analysis (Figure S11d and e in the Supporting Information), which showed the three expected correlation rectangles.

In the same way, six doublets are expected for the three inequivalent methylene groups belonging to the benzyloxy moieties (Figure 12 C). These signals are indeed observed (Figure 11 D; see also the 2D COSY analysis, Figure S11d and f in the Supporting Information).

Lastly, six correlated signals are expected for the six hydroquinone protons belonging to the calixarene (Figure 12 E (blue arrows) and Figure S11 g in the Supporting Information). These signals are indeed observed (Figure 12 F), and pairwise correlated, as expected (see 2D COSY analysis, Figure S11d and g in the Supporting Information).

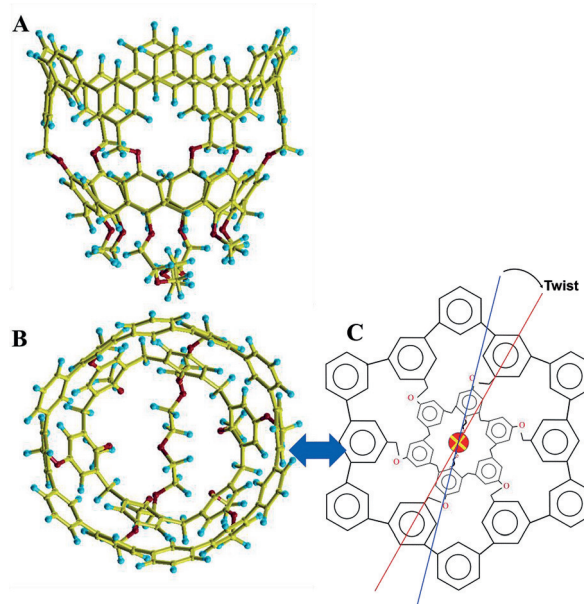


**Figure 11.** DFT-optimised geometry of **15** (side view (A) and top view (B)). C) Simplified in-plane projection of **15** (top view), highlighting the twist angle between the SWCNT short segment stage and the calixarene. Methoxy groups are omitted for clarity and the symmetry axis lying in the centre of the molecule is highlighted as a yellow cross (see the Supporting Information, Figure S11 a).

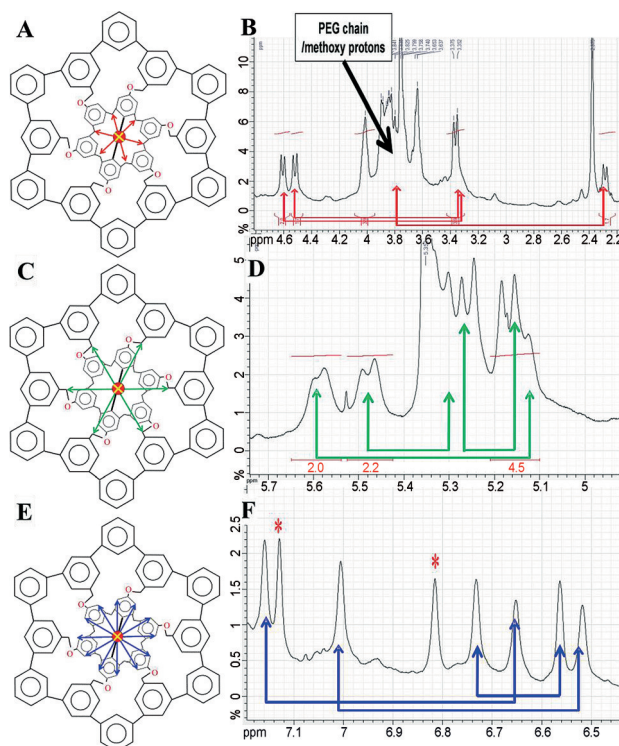


**Figure 12.**  $^1\text{H}$  NMR spectroscopy analysis of **15** at 233 K. Symmetry-induced equivalences (A, red arrows) to explain the three observed doublet of doublets for the bridging methylenes from the calixarene (B). Symmetry-induced equivalences (C, green arrows) to explain the sets of doublet of doublets observed for the benzyloxy groups protons (D). E) Symmetry-induced equivalences (E, blue arrows) to account for the six different hydroquinone signals observed in the  $^1\text{H}$  NMR spectrum (F). Red asterisks: signals belonging to the protons from the SWCNT short segment upper stage.

Extra signals are also observed in the same area (Figure 12F, red asterisks, and Figure S11h in the Supporting Information, red asterisks/red arrows). Analysis of the edited HSQC (Figure S11j in the Supporting Information) and COSY 2D experiments (Figure S11d in the Supporting Information) shows that these signals belong to the *m*-[cyclopoly(phenylene)] ring protons. The extensive overlapping of these signals and the low symmetry of the molecule preclude a more precise assignment.

The four methoxy groups of **15** are observed as two distinct signals (as expected for symmetry reasons) at  $\delta=3.76$  and 2.38 ppm on the  $^1\text{H}$  NMR spectrum (HSQC, Figure S11j in the Supporting Information). The signals belonging to the PEG chain are observed as a complex set of overlapping doublets (Figure S11e and j in the Supporting Information). For all relevant signals, the observed intensity ratios are in good agreement with those expected.

The high-temperature analysis of **15** proved to be difficult because this compound was quite unstable under these conditions. Indeed, fast evolution of the signals was observed upon heating in high-boiling solvents, such as  $[\text{D}_6]\text{DMSO}$ , which was indicative of rapid decomposition. However, compound **15** proved to be stable for a limited period of time (a few hours) at 90 °C in  $[\text{D}_7]\text{DMF}$  under argon (sealed NMR tube).

The evolution of the  $^1\text{H}$  NMR spectrum with temperature under these conditions is shown in Figure 13. Interestingly, the ambient-temperature spectrum in  $[\text{D}_7]\text{DMF}$  (Figure 13, 299 K) appears to be more resolved than the corresponding one in  $\text{CDCl}_3$  (Figure 10A). This shows that the intramolecular motions (sketched in Figure 10C, blue arrows) are faster in  $[\text{D}_7]\text{DMF}$ . As the temperature increases, the signals become sharper.

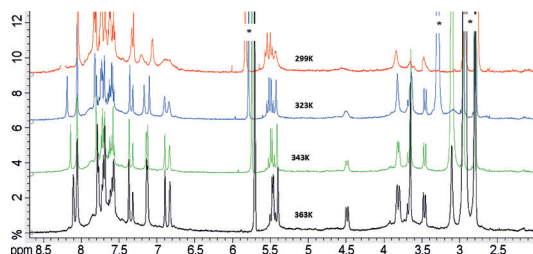


**Figure 13.** Variable-temperature analysis of **15** in  $[\text{D}_7]\text{DMF}$  (solvents marked with asterisks).

At 363 K, the  $^1\text{H}$  NMR spectrum is characteristic of  $C_{2v}$  symmetry (Figure 14A). This is in accordance with faster rotational motion of the two stages of **15** (Figure 10C), resulting in this averaged highly symmetric spectrum (Figure 14A, see also Figure S11k in the Supporting Information). Detailed NMR spectroscopy analysis is fully consistent with this interpretation. For example, at 363 K, two sets of doublets corresponding to the bridging methylenes of the calixarene stage of **15** are observed at  $\delta=2.84/3.69$  and 3.47/4.5 ppm (Figure 14B, red). All other protons show the expected coupling patterns (Figure S11m in the Supporting Information, COSY). The HSQC ex-

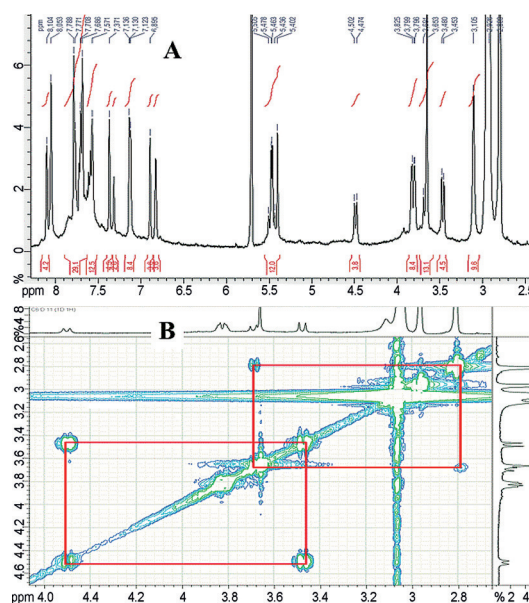


**Figure 14.** A)  $^1\text{H}$  NMR spectrum of **15** at 363 K. B) Magnification of the bridging methylene area of the COSY NMR spectrum.

periment (Figure S11o in the Supporting Information) provides evidence of all expected  $^1\text{H}/^{13}\text{C}$  correlations. All other signals are fully coherent with the proposed structure of **15** (Figure S11l in the Supporting Information). Unfortunately, the limited stability of **15** at high temperature prevented us from performing further analysis.

The identity and purity of **15** were further confirmed by mass spectrometry. Only one signal is observed after purification (Figure S11q and r in the Supporting Information), which is in accordance with the observation of a single spot by TLC. Importantly, the tracking of **15** was made easier by its characteristic V-shaped spot on the silica gel TLC plate.

Along with the short nanotube segments **9**, **6** and **15**, incompletely cyclised by-products are observed. These by-products are the result of deborylation/debromination (Figure S4j in the Supporting Information), Suzuki over-couplings and ligand scrambling (Figures S6q and S11s in the Supporting Information). Although these side reactions are known,<sup>[50–53]</sup> their extent here may be due to the very high number of consecutive Suzuki coupling steps (8, 10 and 12 for **6**, **9**, and **15**, respectively). This makes the complete assembly of the upper SWCNT short segments a slow process, which leaves enough time for such “faults” to occur. This trend is reinforced by the strained nature of **6**, **9**, and **15**. As a consequence, the reaction time was optimised: 10 h for compound **6**, and 6 h for compounds **9** and **15**. These comparatively short reaction times decrease the overall yield, but, most importantly, reduce the amount of faulty products, which results in simpler purification. We indeed observed that these faulty products were difficult to remove.

Extensive DFT calculations were performed on compounds **6**, **9** and **15** (Figure S18 in the Supporting Information). Figures 15, 16 and 17 show the HOMO/LUMO systems of the different SWCNT short segments.

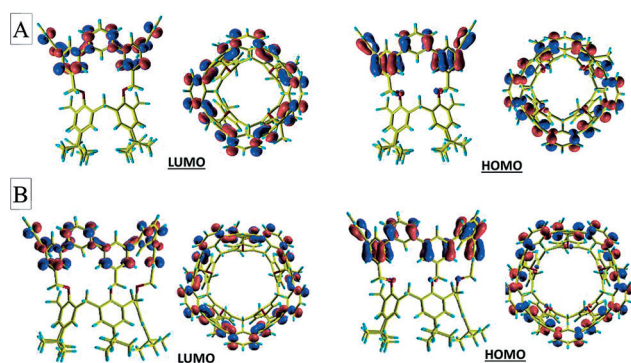


**Figure 15.** DFT-computed LUMOs and HOMOs of the calix[4]arene-derived SWCNT short segment **6** (A) and calix[5]arene-derived SWCNT short segment **9** (B).

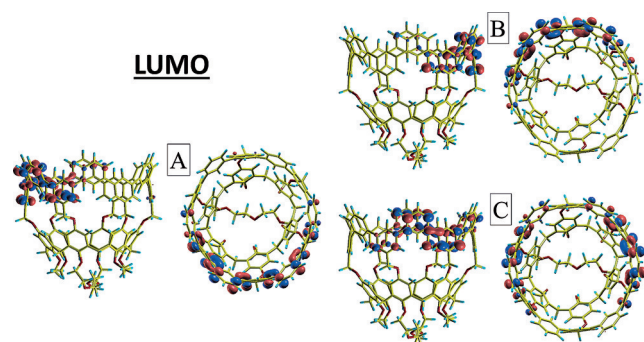


**Figure 16.** DFT-computed LUMOs of the calix[6]arene-derived SWCNT short segment **15**.

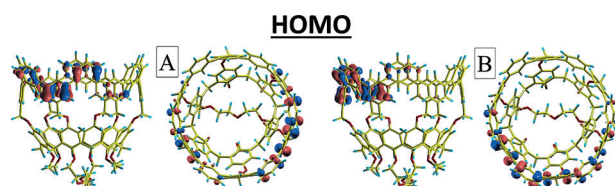


**Figure 17.** DFT-computed HOMOs of the calix[6]arene-derived SWCNT short segment **15**.

Regarding calix[5]-derived segment **9**, the calculations were performed with *t*Bu groups at the *para* position to reduce the calculation time (Figure 15B).

In all three cases, the SWCNT short segments are fully conjugated. The lower symmetry of compound **15** compared with that of **6** and **9** splits the HOMO and LUMO of the corresponding SWCNT short segment into different quasi-degenerate ones. However, the observed overlapping patterns are similar to those observed for **6** and **9**.

Moreover, there are no low-lying orbitals delocalised over both the short SWCNT and calixarene scaffold. This means that the *m*-phenylene and calixarene stages are electronically decoupled. However, their respective energy levels allow for electron/hole transfer upon excitation. Figure S18d in the Supporting Information shows the calculated electronic

structures for **6**, **9** and **12**. An electronic transition in one of these compounds will result in an excited state that will relax very rapidly through charge transfer from/to the other chromophore (Figure S18e in the Supporting Information). Considering the small electronic coupling between the calixarene and *m*-phenylene stages, electron/hole recombination should be disfavoured, resulting in long-lived charge-separated states.

### Synthesis of a functionalised zigzag SWCNT short segment

To really envision the growth of SWCNTs by using our short segments as starting points, the introduction of suitable functional groups is necessary. We thus demonstrated this possibility by a proof-of-concept experiment with the methoxy-functionalised calixarene scaffold **19** (Figure 18).

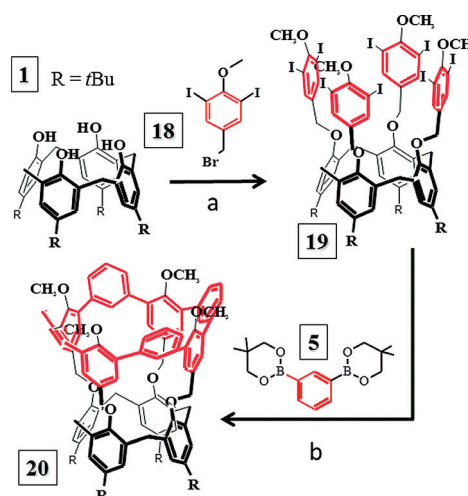


**Figure 18.** Synthesis of a *p*-methoxy-functionalised zigzag SWCNT short segment on a calix[4]arene scaffold.

Key diiodo derivative **18** is easily available on a 20 g scale, starting from inexpensive and commercially available 4-hydroxy-3,5-diiodobenzaldehyde (Figures S12–S15 in the Supporting Information). From octaiodo scaffold **19** (Figure S16 in the Supporting Information), the corresponding SWCNT short segment **20** was obtained under similar conditions to those used for **9** and **15** (Figure S17 in the Supporting Information). This proof-of-concept experiment shows that, in our case, the steric effects associated with the presence of substituents next to the reactive sites do not prevent the final cyclisation steps. It could thus open up the way to synthesise lengthened SWCNT segments, for example, by means of a demethylation/triflation/Suzuki coupling sequence. Other, more easily removed, protecting groups than methyl may also be envisioned. This could allow the introduction of extra aromatic units, oriented parallel (e.g., linear *p*-poly(phenylene)-type oligomers), for the construction of longer tubes. This should open up, for the first time, simple strategies for the synthesis of arbitrarily long SWCNTs; a fundamental improvement compared with the previously envisioned lengthening strategies for SWCNT short segments.

## Conclusion

We described the first synthesis of short segments of zigzag-type CNTs with tuned diameters. In the case of the calix[4]arene scaffold, this approach involved a very simple two-step protocol, starting from cheap, commercially available reagents. This strategy appeared to be far simpler than those previously described.<sup>[17–24,29]</sup> Our synthetic strategy is extremely versatile because it opens up the possibility of using a huge variety of bis(boronic)derivatives in combination with different calixarene scaffolds. This opens up the way to synthesise new families of macrocyclic compounds, with well-defined diameters and constrained into unconventional tubular geometries. DFT calculations show that these compounds should exhibit interesting photophysical properties. It should also be underlined that compound **15** exhibits (to the best of our knowledge) the largest rigid cavity known so far for a calixarene derivative, which is interesting for supramolecular chemistry.

Apart from its “scaffolding” effect, the calixarene stage itself provides interesting possibilities for the future synthesis of original SWCNT/calixarene composites, combining the properties of both families of compounds. For example, it seems reasonable to consider that the presence of the calixarene fragment will confer ion complexation capacities on our SWCNT short segment/calixarene composites (especially for **15**, with its PEG chain). At the same time, the very large diameter of the SWCNT short segment will make these compounds interesting hosts for large-molecule complexation. These two effects pave the way to interesting ion-pair complexation effects for large molecules (biology) that cannot be addressed with current calixarene receptors, with comparatively smaller cavities.

As a longer term prospect, our strategy for the lengthening of SWCNT short segments should result in very interesting SWCNT/calixarene composites, with only one calixarene unit at one end. Providing that ions are then complexed into these units, this will result in a completely new object, that is, a SWCNT with only a single charge (if alkaline ions are used) at one end. This will lead to new possibilities for the organisation of these nanotubes on surfaces, for example, on electrically polarised substrates or by using polyelectrolytes.

Finally, we obtained the first functionalised zigzag SWCNT short segments. The functionalisation pattern and symmetry allow for simple strategies to be envisioned for lengthening. This may lead to the total synthesis of arbitrarily long segments by simple iterative approaches. This work is in progress within our group and will be reported in due course.

## Experimental Section

Experimental details are provided in the Supporting Information.

## Acknowledgements

E.A. and B.B. gratefully acknowledge the French Ministry of Research for PhD thesis grants. We thank the French National

Agency for Research (ANR) for funding, grant number ANR-08-JCJC-0085.

**Keywords:** calixarenes · carbon · nanotubes · macrocycles · total synthesis

- [1] M. Monthieux, V. Kuznetsov, *Carbon* **2006**, *44*, 1621.
- [2] S. Iijima, *Nature* **1991**, *354*, 56.
- [3] S. Iijima, T. Ichihashi, *Nature* **1993**, *363*, 603.
- [4] D. S. Bethune, C. H. Kiang, M. S. de Vries, G. Gorman, R. Savoy, J. Vazquez, R. Beyers, *Nature* **1993**, *363*, 605.
- [5] R. Martel, T. Schmidt, H. R. Shea, T. Hertel, P. Avouris, *Appl. Phys. Lett.* **1998**, *73*, 2447.
- [6] S. J. Tans, A. R. M. Verschueren, C. Dekker, *Nature* **1998**, *393*, 49.
- [7] P. Bondavalli, P. Legagneux, D. Pribat, *Sensors and Actuators B* **2009**, *140*, 304.
- [8] R. Saito, M. Fujita, G. Dresselhaus, M. S. Dresselhaus, *Appl. Phys. Lett.* **1992**, *60*, 2204.
- [9] S. M. Bachilo, L. Balzano, J. E. Herrera, F. Pompeo, D. E. Resasco, R. B. Weisman, *J. Am. Chem. Soc.* **2003**, *125*, 11186.
- [10] X. Li, X. Tu, S. Zaric, K. Welscher, W. S. Seo, W. Zhao, H. Dai, *J. Am. Chem. Soc.* **2007**, *129*, 15770.
- [11] M. He, A. I. Chernov, P. V. Fedotov, E. D. Obraztsova, J. Sainio, E. Rikkinen, H. Jiang, Z. Zhu, Y. Tian, E. I. Kauppinen, M. Niemelä, A. O. I. Krause, *J. Am. Chem. Soc.* **2010**, *132*, 13994.
- [12] L. Ding, A. Tselev, J. Wang, D. Yuan, H. Chu, T. P. McNicholas, Y. Li, J. Liu, *Nano Lett.* **2009**, *9*, 800.
- [13] S. Ghosh, S. M. Bachilo, R. B. Weisman, *Nat. Nanotechnol.* **2010**, *5*, 443.
- [14] X. Tu, S. Manohar, A. Jagota, M. Zheng, *Nature* **2009**, *460*, 250.
- [15] T. Tanaka, H. Jin, Y. Miyata, S. Fujii, H. Suga, Y. Naitoh, T. Minari, R. Miyadera, K. Tsukagoshi, H. Katura *Nano Lett.* **2009**, *9*, 1497.
- [16] M. C. Hersam, *Nat. Nanotechnol.* **2008**, *3*, 387.
- [17] S. Hitosugi, W. Nakanishi, T. Yamasaki, H. Isobe, *Nat. Commun.* **2011**, *2*, 492.
- [18] H. Omachi, Y. Segawa, K. Itami, *Org. Lett.* **2011**, *13*, 2480.
- [19] S. Hitosugi, T. Yamasaki, H. Isobe, *J. Am. Chem. Soc.* **2012**, *134*, 12442.
- [20] R. Jasti, J. Bhattacharjee, J. B. Neaton, C. R. Bertozzi, *J. Am. Chem. Soc.* **2008**, *130*, 17646.
- [21] R. Gleiter, B. Esser, S. C. Kornmayer, *Acc. Chem. Res.* **2008**, *41*, 1108.
- [22] T. J. Sisto, M. R. Golder, E. S. Hirst, R. Jasti, *J. Am. Chem. Soc.* **2011**, *133*, 15800.
- [23] Y. Segawa, S. Miyamoto, H. Omachi, S. Matsuura, P. Šenel, T. Sasamori, N. Tokitoh, K. Itami, *Angew. Chem. Int. Ed.* **2011**, *50*, 3244; *Angew. Chem.* **2011**, *123*, 3302.
- [24] S. Yamago, Y. Watanabe, T. Iwamoto, *Angew. Chem. Int. Ed.* **2010**, *49*, 757; *Angew. Chem.* **2010**, *122*, 769.
- [25] T. Nishiuchi, X. Feng, V. Enkelmann, M. Wagner, K. Müllen, *Chem. Eur. J.* **2012**, *18*, 16621.
- [26] H. Omachi, T. Nakayama, E. Takahashi, Y. Segawa, K. Itami, *Nat. Chem.* **2013**, *5*, 572.
- [27] F. E. Golling, M. Quernheim, M. Wagner, T. Nishiuchi, K. Müllen, *Angew. Chem. Int. Ed.* **2014**, *53*, 1525; *Angew. Chem.* **2014**, *126*, 1551.
- [28] E. Kayahara, V. K. Patel, S. Yamago, *J. Am. Chem. Soc.* **2014**, *136*, 2284.
- [29] B. Esser, F. Rominger, R. Gleiter, *J. Am. Chem. Soc.* **2008**, *130*, 6716.
- [30] A. M. Butterfield, B. Gilomen, J. S. Siegel, *Org. Process Res. Dev.* **2012**, *16*, 664.
- [31] L. T. Scott, E. A. Jackson, Q. Zhang, B. D. Steinberg, M. Bancu, B. Li, *J. Am. Chem. Soc.* **2012**, *134*, 107.
- [32] U. H. F. Bunz, S. Menning, N. Martin, *Angew. Chem. Int. Ed.* **2012**, *51*, 7094; *Angew. Chem.* **2012**, *124*, 7202.
- [33] J. Xia, M. R. Golder, M. E. Foster, B. M. Wong, R. Jasti, *J. Am. Chem. Soc.* **2012**, *134*, 19709.
- [34] T. J. Sisto, X. Tian, R. Jasti, *J. Org. Chem.* **2012**, *77*, 5857.
- [35] A. Yagi, Y. Segawa, K. Itami, *J. Am. Chem. Soc.* **2012**, *134*, 2962.
- [36] H. Ito, Y. Mitamura, Y. Segawa, K. Itami, *Angew. Chem. Int. Ed.* **2015**, *54*, 156; *Angew. Chem.* **2015**, *127*, 161.
- [37] M. R. Golder, R. Jasti, *Acc. Chem. Res.* **2015**, *48*, 557.
- [38] P. J. Evans, E. R. Darzi, R. Jasti, *Nat. Chem.* **2014**, *6*, 404.
- [39] H. A. Staab, F. Binnig, *Chem. Ber.* **1967**, *100*, 293.

- [40] T. Yamamoto, Y. Hayashi, A. Yamamoto, *Bull. Chem. Soc. Jpn.* **1978**, *51*, 2091.
- [41] K. N. Trueblood, C. B. Knobler, E. Maverick, R. C. Helgeson, S. B. Brown, D. J. Cram, *J. Am. Chem. Soc.* **1981**, *103*, 5594.
- [42] D. J. Cram, T. Kaneda, R. C. Helgeson, G. M. Lein, *J. Am. Chem. Soc.* **1979**, *101*, 6752.
- [43] J. Y. Xue, K. Ikemoto, N. Takahashi, T. Izumi, H. Taka, H. Kita, S. Sato, H. Isobe, *J. Org. Chem.* **2014**, *79*, 9735.
- [44] A. Casnati, P. Jacopozzi, A. Pochini, F. Ugozzoli, R. Cacciapaglia, L. Mandolini, R. Ungaro, *Tetrahedron* **1995**, *51*, 591.
- [45] K. Iwamoto, K. Araki, S. Shinkai, *J. Org. Chem.* **1991**, *56*, 4955.
- [46] V. Huc, V. Guérineau, *Eur. J. Org. Chem.* **2010**, *11*, 2199.
- [47] V. Huc, E. Npetgat, V. Guérineau, S. Bourcier, A. Dos Santos, R. Guillot, J. P. Baltaze, C. Martini, *Eur. J. Org. Chem.* **2010**, *11*, 6186.
- [48] S. V. Shorunova, M. M. Krayushkin, F. M. Stoyanovich, M. Irie, *Russ. J. Org. Chem.* **2006**, *42*, 1490.
- [49] M. Baur, M. Frank, J. Schatz, F. Schildbach, *Tetrahedron* **2001**, *57*, 6985.
- [50] S. Kappaun, M. Zelzer, K. Bartl, R. Saf, F. Stelzer, S. Slugovc, *J. Polym. Sci.: Part A: Polym. Chem.* **2006**, *44*, 2130.
- [51] S. T. Handy, H. Bregman, J. Lewis, X. Zhang, Y. Zhang, *Tetrahedron Lett.* **2003**, *44*, 427.
- [52] O. Navarro, H. Kaur, P. Mahjoor, S. P. Nolan, *J. Org. Chem.* **2004**, *69*, 3173.
- [53] B. Hohl, L. Bertschi, X. Zhang, A. D. Schlüter, J. Sakamoto, *Macromolecules* **2012**, *45*, 5418.

---

Received: September 14, 2015

Revised: November 6, 2015

Published online on January 27, 2016